

Anti-biofouling organic-inorganic hybrid membrane for water treatment†

Ajay K. Singh,^a Priyanka Singh,^b Sandhya Mishra^b and Vinod K. Shahi^{*a}

Received 30th August 2011, Accepted 25th October 2011

DOI: 10.1039/c1jm14250j

Biofouling is a critical problem in membrane filtration processes. Herein, we report an anti-biofouling organic-inorganic hybrid membrane for water treatment. Antimicrobial drug (substituted 1,3,4-oxadiazole) with functionalized silica were successfully incorporated into organic phase by sol-gel in aqueous media followed by formal cross-linking to achieve highly stable and anti-biofouling membrane. Structural features of these phosphonic acid functionalized hybrid membranes depended on silica content. Physicochemical properties of prepared membranes revealed their stable (thermal, mechanical, and chemical), chlorine tolerance and charged nature. The most suitable membrane (MO-6) exhibited better performance in comparison to reported membranes. Absence of any deterioration in membrane permeability after 30 days operation under *E. coli* broth solution, confirmed their anti-biofouling nature.

Introduction

Water contamination is a world-wide problem, and human health has been heavily affected by poor water quality and water related diseases.¹ An urgent need in the 21st century is access to secure, sustainable sources of fresh water.² Membrane based water desalination/purification technologies have a wide range of advantages in comparison to traditional separation methods. These are embedded with key features like low energy consumption, easy integration as well as scale-up.³ Nanofilter (NF) membranes reject larger solutes (1–10 nm) *via* size exclusion, are suitable for water desalination/purification of ground water. Several polymer synthesis and surface modification strategies were explored to achieve nanoporous membranes.^{4–7} Generally, NF membranes are derived from either polyamide or poly(ether sulfone) but they are chemically instable in the presence of sanitizing agents, especially chlorine,⁸ which is generally used for preventing bacteriological contamination of potable water. Furthermore, the unprotected membrane is itself susceptible to fouling (organic fouling, colloidal fouling, and biofouling). Among all types of fouling, formation of bio-film on the membrane surface (biofouling) is a pervasive problem for material architecture.^{9,10}

Biofouling has severe adverse impacts, and autopsy studies of fouled membranes (NF used during water desalination/treatment) exhibited more than 50% (w/w) of dry fouling layers, which was of biological origin.^{11,12} Unlike other sources of fouling, biofouling cannot be reduced by pretreatment, because of its self-replicating nature. Generally, three strategies: biocide dosing (continuous or intermittent), chemical or physical cleaning procedures, and developing the membrane prone to biofouling, were adopted to avoid biofouling. Antimicrobial membranes prone to biofouling for water treatment pose particular challenges because of its architecture (pore size, surface roughness and charged nature), along with chemical, mechanical and hydraulic stabilities. A variety of polymers including polysiloxanes and other silicon based materials, were used for health care¹³ and biomedical products,^{14–16} because of their cytotoxicity and desirable physical properties.¹⁷ Organic/inorganic nanocomposites are generally organic polymer composites with inorganic nanoscale building blocks, which combine the advantages of the inorganic material (*e.g.*, rigidity, thermal stability) and the organic polymer (*e.g.*, flexibility, dielectric, ductility, and processability).^{18–20} In addition, compounds bearing 1,3,4-oxadiazole ring showed antibacterial and antifungal activity.^{21,22} Thus, there is great opportunity for developing organic-inorganic hybrid membranes, containing substituted 1,3,4-oxadiazole and silica. These membranes are expected to exhibit antimicrobial activity, good performance and stabilities.

In this work, we are reporting phosphonic acid grafted organic-inorganic nanocomposite membrane derived by acid catalyzed sol-gel in aqueous media, containing substituted 1,3,4-oxadiazole ring. Reported membranes were antimicrobial in nature (avoid biofilm formation) and exhibited good stabilities (thermal, mechanical, dimensional and chemical). Poly(vinyl

^aElectro-Membrane Processes Division, Central Salt & Marine Chemicals Research Institute, Council of Scientific & Industrial Research (CSIR), G. B. Marg, Bhavnagar, 364002, Gujarat, INDIA. E-mail: vkshahi@cscri.org; vinodshahi1@yahoo.com; Fax: +91-278-2567562/2566970; Tel: +91-278-2569445

^bSalt and Marine Chemicals Division, Central Salt & Marine Chemicals Research Institute, Council of Scientific & Industrial Research (CSIR), G. B. Marg, Bhavnagar, 364002, Gujarat, INDIA

† Electronic supplementary information (ESI) available. See DOI: 10.1039/c1jm14250j

alcohol) (PVA) was used to achieve chlorine tolerance nature of these membranes, because acetalization of oxidative sensitive primary alcohol groups by formal reaction (cross-linking), which lead to more stable ether-type linkages. Furthermore, good flux, salt rejection, and absence of fouling of these membranes, revealed their potential application for water desalination.

Experimental

Materials

Aminopropyltriethoxysilane (APTEOS) (99%) were obtained from Sigma-Aldrich chemicals and used as received. Poly(vinyl alcohol) (MW: 125 000), formaldehyde (37% in water), phosphorous acid, hydrochloric acid, sulfuric acid, *p*-chloro benzoic acid, hydrazine hydrate, sodium hydroxide, sodium chloride, sodium hypochlorite, *N*-methyl pyrrolidone, dimethylformamide, hexane, iodine crystal, magnesium turnings, tetrahydrofuran (THF), acetone and methanol were obtained from S. D. Fine Chemicals, Mumbai, India. Solvents were used after proper distillation, while double distilled water was used for experiments.

Synthesis of siloxane monomer 3-((4-(5-(2-((3-aminopropyl) diethoxysilyl)ethylthio)-1,3,4-oxadiazol-2-yl)phenyl) diethoxysilyl)propan-1-amine (APDSMO)

Synthesis of 2-(2-chloroethylthio)-5-(4-chlorophenyl)-1,3,4-oxadiazole was achieved through multisteps (Fig. 1), while APDSMO was synthesized by Barbier-Grignard reaction using APTEOS.²³ The general preparation method: to a three-necked, 250 mL round-bottom flask equipped with a magnetic stirrer,

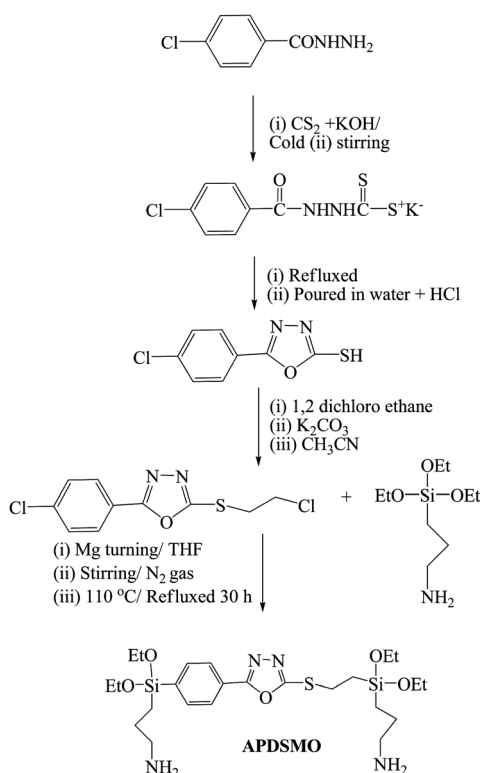


Fig. 1 Synthesis route for siloxane monomer (APDSMO).

nitrogen inlet, drying tube, condenser, and addition funnel, a mixture of Mg turning (1.5) and APTEOS (44.4 mL; 0.2 mol) in THF (30 mL) and a crystal of iodine was added. The reaction mixture was refluxed under constant stirring. Then 2-(2-chloroethylthio)-5-(4-chlorophenyl)-1,3,4-oxadiazole (5.5 g; 2 mmol) in THF (20 mL) was drop-wise added over 30 min. After 10 h refluxing at constant stirring, greenish yellow colour viscous liquid was obtained. The mixture was cooled to room temperature and THF was removed by vacuum rotatory evaporator. 30 mL hexane was added to obtained viscous liquid followed by filtration and drying under vacuum to obtain yellow coloured liquid. Yield: 63% Anal. calcd for $[C_{28}H_{44}N_4O_5Si_2]$ (572.84): C, 58.70; H, 7.74; N, 9.76; Si, 9.81 Found: C, 58.68; H, 7.72; N, 9.71; Si, 9.80. Obtained yellow coloured liquid was highly hygroscopic and turned glass like solid polysiloxane (hydrolysed APDSMO) due to hydrolysis within three days.

Preparation of hybrid membranes

10 wt% of PVA solution (aq.) was prepared in water under refluxed conditions at 70 °C for 4 h. Solution was filtered and the desired amount of APDSMO was added under constant stirring for 6 h. Solution was transformed into gel by adding 2 mL 1 M HCl. Mixture was stirred at room temperature for 6 h. Obtained viscous gel was transformed into thin film on cleaned glass plate. After 30 min drying at room temperature, thin film was precipitated (gelated) in hexane (10 °C) to create nano porous structure.²⁴ Precipitated thin film was dried at room temperature for 24 h, followed at 80 °C for 24 h under vacuum oven. Obtained films were subjected for effective cross-linking by using formaldehyde solution (2.5 wt%) and conc. H_2SO_4 for 3 h at 60 °C. Cross-linked membranes were dipped in methanol to remove residual formaldehyde solution. Obtained membranes were subjected to phosphorylation using 1 : 1 (w/w) formaldehyde and phosphorus acid,²³ for 3 h at 70 °C. Thickness ($100 \pm 10 \mu m$) of cross-linked membrane was measured by digital micrometre. Different prepared membranes were designated as MO-X, where 10X is the weight percentage of APDSMO in the membrane matrix.

Instrumental characterizations of the APDSMO and membranes

FTIR spectra of dried membrane samples were obtained by Spectrum GX series 49387 spectrometer in the range of 4000–700 cm^{-1} . The IR spectrum for a synthesized intermediate was obtained by the KBr pellet method. Wide angle X-ray diffractograms of MO-X membranes were recorded using Philips Xpert X-ray diffractometer with $Cu-K\alpha(1.54056)$ radiation. 1H and ^{13}C NMR spectrometer (Bruker 500 MHz) in a D_2O and d_6 -DMSO solvent, were used.

The thermal degradation of MO-X membranes was investigated by thermo-gravimetric analyzer (Mettler Toledo TGA/SDTA851 with Star software) under a nitrogen atmosphere with 10 °C min^{-1} heating rate from 30 to 450 °C. Differential scanning calorimetry (DSC) measurement was also carried out with heating rate 5 °C min^{-1} (30–450 °C). The dynamic mechanical stabilities of MO-X membranes were evaluated by Mettler Toledo dynamic mechanical analyzer 861 instruments with Star software under nitrogen with 10 °C min^{-1} heating rate (30 to 320 °C) to investigate the effect of silica content on membrane mechanical stability.

Transmission electron microscope (TEM) analysis for dried MO-X membranes was performed by a JEOL 1200EX. The JEOL 1200EX TEM with tungsten was operated at an accelerating voltage of up to 120 kV. Atomic force microscopy (AFM) images of dried membranes were recorded by NTEGRA AURA (NTMDT) in semi-contact mode SPM NSG with 01 tip (radius of curvature: 10 nm, natural frequency for the cantilever was 300 kHz) to determine the surface roughness. In this measurement mode, cantilever, where the tip was located, oscillated with its natural frequency. Sample topography was obtained by oscillation amplitude. For scanning electron microscopy (SEM), gold sputter coatings were carried out on desired membrane samples at pressure ranging between 1 and 0.1 Pa. Sample was loaded in the machine, operated at 10^{-2} to 10^{-3} Pa vacuum with EHT 15.00 kv with 300 V collector bias. SEMs were recorded by Leo microscope. The optical densities of microbial solutions were evaluated by using a VARIAN 50 bio UV-Vis spectrophotometer.

Membrane flux, solute rejection and chemical stabilities

Water flux across nanocomposite membranes were measured in a two compartment cell separated by circular membrane disk (4.0 cm^2) placed at the bottom of the cell with top active layer towards the feed solution. Feed compartment was well stirred by mechanical stirrer (300 rpm).²⁵ Membranes were sealed between a Teflon O ring and a stainless steel porous support. Varied pressure (0.62–0.9 MPa) was applied on feed side using N_2 cylinder for estimation of permeate flux and salt rejection by following eqn (1), (2).

$$\text{Flux} (\text{l. m}^{-2}. \text{h}^{-1}) = \frac{\text{permeate } (l)}{\text{membrane area } (\text{m}^2). \text{time } (h)} \quad (1)$$

$$\text{Rejection } (\%) = \left(1 - \frac{\text{permeate conductance}}{\text{feed conductance}} \right) \times 100 \quad (2)$$

Membrane stability was assessed in different solvents, different acids with varied concentration, base and NaOCl (chlorine stability) and weight loss (W_1) was estimated by the following equation:

$$W_1 = \left[1 - \frac{W_{\text{dry}}}{W_s} \right] \times 100 \quad (3)$$

Where, W_{dry} and W_s are the weight of dry and chemically treated dry membranes.

Microbial activity

Antimicrobial properties of APDSMO, polysiloxane and MO-X membranes were tested for water-borne fungi (*Aspergillum niger*) and bacteria (*Escherichia coli*). All antifungal and antibacterial tests were performed in triplicate to ensure reproducibility. Standard testing protocol for water insoluble antimicrobials was used following the bio-safety rule, included in ESI (S1†).²⁶

Antibacterial activity

Synthesized APDSMO, hydrolysed APDSMO and MO-X membranes were screened for their antibacterial activity against one bacterium (*E. coli*) by three different ways: i. zone of

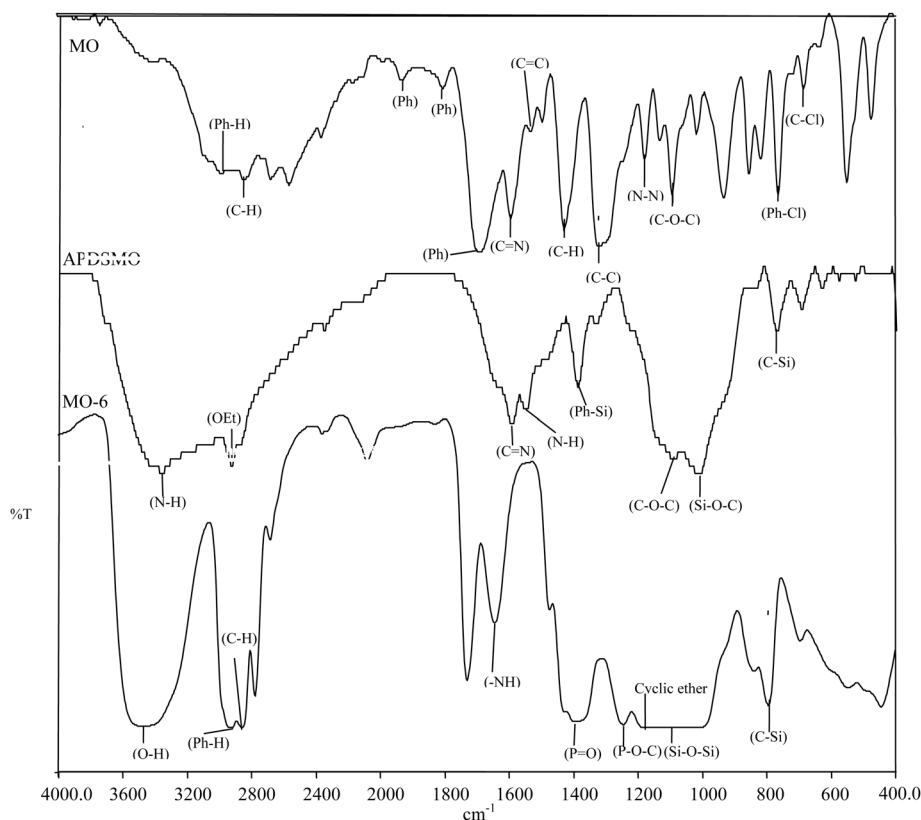


Fig. 2 FTIR spectra of: (a) 2-mercaptoethane-5-phenyl-1,3,4-oxadiazole (MO); (b) APDSMO; and (c) MO-6.

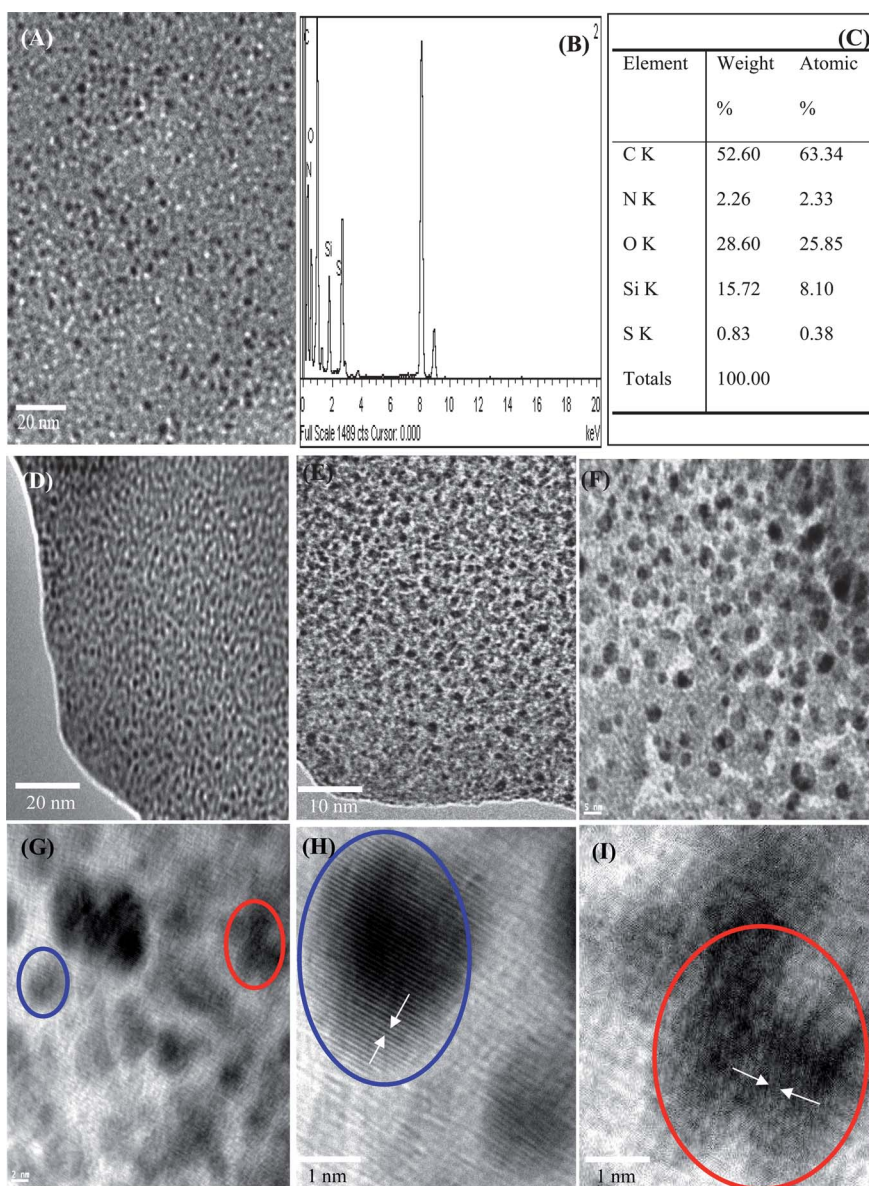


Fig. 3 TEM images of: (A) uncross-linked MO-6 (without phosphorylation); (B, C) EDX data and table for elemental analysis of uncross-linked MO-6 (without phosphorylation); (D,E,F,G,H,I) cross-linked MO-6 membrane at different magnification mode.

inhibition (mm); ii. growth of inhibition (%); and iii. minimum inhibitory concentration (MIC) ($\mu\text{g ml}^{-1}$).

[i] Zone of inhibition (mm). The disc diffusion method was used to screen the antibacterial activity against coliform bacteria *E. coli*. *E. coli* culture (100 μl , with OD_{600} : 2.3299) was evenly spread over the surface of double layer Luria Base (LB) agar plates. The double layer was formed by pouring a layer of hard agar (2.5%) overlapping with the layer of soft agar (0.7%), which allowed solidifying; thereafter wells were drilled in LB plates. Different amount APDSMO and hydrolysed APDSMO were used for wells on agar plate in such a manner that the copolymer does not spread out. In the case of membranes, the membrane was cut in square pieces (1 cm^2) and pasted on surface of agar. The plates were then incubated at 37 $^{\circ}\text{C}$ for different time

intervals (24, 48, and 72 h) and observed zone of inhibition was measured by Vernier callipers.

[ii] Growth of inhibition. Aqueous solution of APDSMO with different concentrations (5000, 1000, 100, 10 $\mu\text{g ml}^{-1}$) was prepared. 1 mL solution was poured in presterilised petridishes followed by immediate addition of 9 mL of nutrient agar medium. Each dish was kept on auto-rotator to achieve thorough mixing of medium and compound. Afterward, fungus and bacterial strain were inoculated in the dishes (diameter 5 mm) and growth of inhibition was estimated by the following equation.

$$\% \text{ growth inhibition} = \left[1 - \frac{t_d}{c_d} \right] \times 100 \quad (4)$$

Where c_d is the colony diameter of treated set and t_d is the colony diameter of control set.

[iii] Determination of MIC. MIC was determined against coliform bacteria *E. coli*. *E. coli* culture (OD_{600} : 2.3299) was inoculated into LB broth containing different concentration of APDSMO, hydrolysed APDSMO, and membranes (obtained solution OD were maintained at 1.000 ± 0.001 by adding sterile water). Negative control tubes contained only inoculated broth (after 24 h in rotating shaker (37 °C, 220 rpm)) and turbidity of tubes was noted before and after incubation.

Antifungal activity

Fungal growth inhibition was also measured in a similar fashion as discussed above. All antifungal and antibacterial tests were performed in triplicate for reproducibility.

Results and discussion

Physical structure of APDSMO and hybrid membranes

Guide peaks in FTIR spectra of MO (2-mercaptoethane-5-phenyl-1,3,4-oxadiazole), APDSMO and MO-6 membrane (Fig. 2) confirms reaction between 5-(4-chlorophenyl)-1,3,4-oxadiazole-2-thiol and 1,2-dichloroethane in presence of weak base and formation of MO. Compound MO showed two medium intensity bands at *ca.* 760 and 681 cm^{-1} ($\nu(\text{Ph}-\text{Cl})$ and $\nu(\text{C}-\text{Cl})$). After Barbier-Grignard reaction, new bands were observed at *ca.* 1390 and 795 cm^{-1} ($\nu(\text{Si}-\text{Ph})$ and $\nu(\text{Si}-\text{C})$ vibration band). Presence of oxadiazole ring in MO and APDSMO was confirmed by the strong intensity band at *ca.* 1088 and 1090 cm^{-1} (C–O–C stretching vibration).²⁷ APDSMO spectra showed two medium intensity bands at *ca.* 3350–3400 cm^{-1} and 1549 cm^{-1} ($\nu(\text{N}-\text{H})$) and a medium intensity band at *ca.* 1590 cm^{-1} ($\nu(\text{C}=\text{N})$) of oxadiazole ring).²⁷ For MO-6 membrane, broad band at *ca.* 1300–1400 cm^{-1} and strong band at *ca.* 1649 cm^{-1} indicated phosphorylation of –NH group, which was further confirmed by the medium intensity band at *ca.* 1245 cm^{-1} ($\nu(\text{P}-\text{O}-\text{C})$). Absorption bands at around 1100 cm^{-1} are characteristic bands for Si–O–Si asymmetrical stretching vibration. Bands at about 1178 cm^{-1} (–C–O–C– stretching vibration for acyclic ether ring of PVA), showed formal cross-linking with formaldehyde. These IR results confirmed formation of phosphonic acid functionalized cross-linked organic-inorganic nanostructure membrane.

¹H NMR spectra for reaction intermediate (5-(4-chlorophenyl)-1,3,4-oxadiazole-2-thiol (COT)), MO and APDSMO were recorded in *d*₆-DMSO (Fig. S1, ESI†). COT exhibited signals at 7.59, 7.94 (phenyl ring protons) and 3.5 ppm (thione-thiol form of mercapto oxadiazole ring). In the presence of base, COT reacted with 1,2-dichloroethane and formed MO (signals at 2.08, 3.35 ppm). This was characterized in ethyl proton and two other signals at 7.58 and 7.93 ppm for phenyl ring protons. After the Barbier-Grignard reaction, signals of phenyl ring protons shifted to 7.35 and 7.87 ppm. This up field shifting indicated shielding of protons due to bonding of electronegative atom (Si) with phenyl ring.

¹³C NMR spectra for APDSMO were recorded in D₂O (Fig. S2, ESI†) and presence of oxadiazole and phenyl ring was

confirmed by the signals at δ value 168.4, 168.1 and 138.1, 136.6, 132.0, 129.8 ppm. In APDSMO, carbon signal at 58 ppm suggested presence of –OCH₂CH₃ group. On the basis of spectral analysis structure for APDSMO and hybrid membrane was proposed (Fig. 1 and Fig. S3(ESI†)).

TEM images for uncross-linked and cross-linked MO-6 membrane and EDX analysis data (Fig. 3) revealed homogeneous distribution of silica in membrane matrix. High organic (PVA) content and relatively large amino propyl group created worm like arrangement in the matrix. TEM images showed two types of silica (crystalline and amorphous) in the membrane matrix. High resolution TEM (Fig. S3(a) ESI†) showed 0.22–0.31 nm crystal lattice spacing (in close agreement with crystalline silicone).²⁸ Size of silica particles were estimated about 2–10 nm (Fig. 3). Black shadows (Fig. S3(b) ESI†) indicate silica particles (SiO₂), while strips (Fig. 5a) represents lattice fringes due to formation of crystalline silica (SiO₂). With increase in APDSMO content in the membrane matrix (reduction in PVA content), crystalline region reduced due to favourable conditions for formation of Si–O–C bonds (availability of more Si). WXR data for hydrolysed APDSMO, hybrid membranes, also confirmed amorphous silica (Fig. S4, ESI†). SEM images (cross-section) for MO-3 hybrid membrane (Fig. 4(a)), showed condensed gill type of arrangement (for top portion) and dense

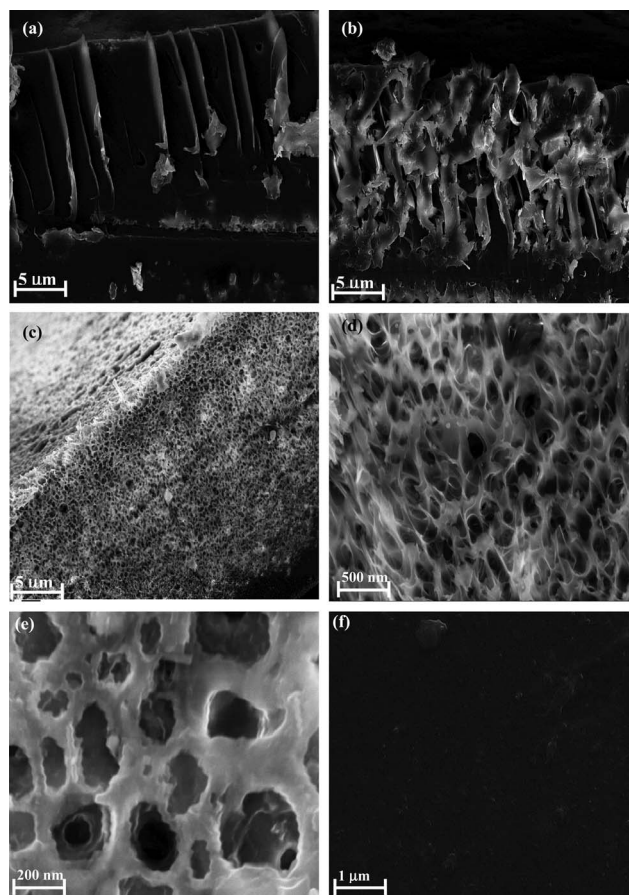


Fig. 4 SEM images of: (a) MO-3 membrane (cross-section); (b) MO-5 membrane (cross-section); (c) MO-6 membrane (cross-section); (d) MO-6 membrane (cross-section) at high resolution; (e) MO-6 membrane (upper portion); and (f) MO-6 membrane (lower portion).

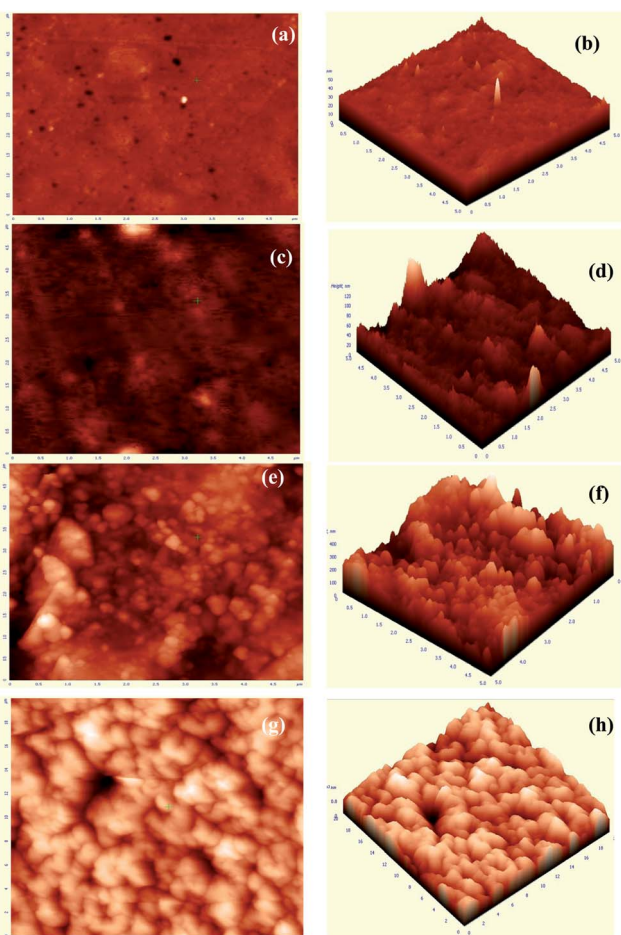


Fig. 5 AFM images for: (a) pristine PVA film; (b) pristine PVA film (3D image); (c) MO-3 membrane; (d) MO-3 membrane (3D image); (e) MO-5 membrane; (f) MO-5 membrane (3D image); (g) MO-6 membrane; and (h) MO-6 membrane (3D image).

layer (bottom). Structural features of hybrid membranes changed with APDSMO content in the membrane matrix (Fig. 4(b–c)). SEM images of APDSMO (Fig. S5 (b) ESI†) looked like termite mounds.

Surface roughness of membranes is an important property to avoid membrane fouling. AFM study was used to estimate membrane surface roughness in semi-contact mode. Obtained AFM images (Fig. 5) showed conglomeration of APDSMO due to polycondensation, which further increased with silica content in membrane matrix. Uncross-linked PVA thin film exhibited lowest surface roughness ($0.03 \mu\text{m}$), while 0.254 , 0.112 , and $0.05 \mu\text{m}$ surface roughness were observed for MO-3, MO-4 and MO-6 hybrid membranes, respectively. With incorporation of

Table 1 Membrane IEC, surface charge concentration (χ^m) values, and volume fraction of water (ϕ_w)

Membrane	IEC	χ^m	ϕ_w
MO-6	1.42	3.5929	0.3490
MO-5	1.28	2.2933	0.2486
MO-4	1.12	2.4521	0.1624
MO-3	0.89	2.2862	0.1192

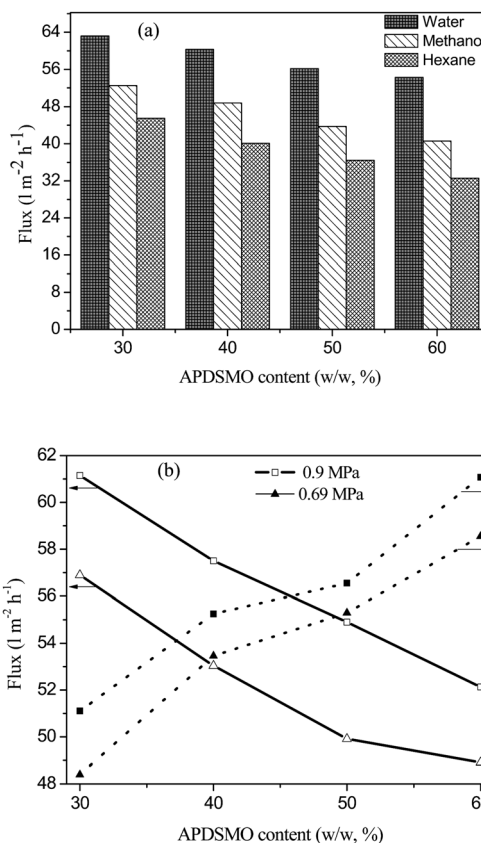


Fig. 6 (a) Flux of hybrid membranes for different solvent at 0.9 MPa applied pressure, (b) variation of flux and solute rejection for different hybrid membrane for NaCl solution (1 g l^{-1}) at different applied pressure.

APDSMO, surface roughness initially increased (MO-3), and beyond 30% (w/w) APDSMO content surface roughness reduced (MO-4, MO-6).

Thermal, mechanical and chemical stabilities of hybrid membranes

Thermal stability of hybrid membranes were analysed by thermogravimetric analysis (TGA) (Fig. S6, ESI†) and two steps

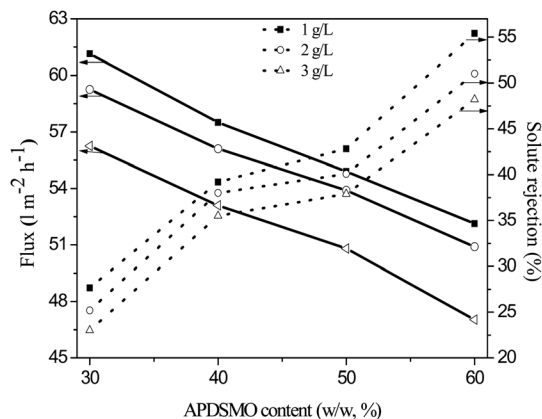


Fig. 7 Variation of flux and solute rejection of different hybrid membranes at 0.9 MPa applied pressure for NaCl of different concentrations.

Table 2 Comparative test results for nanofiltration membrane

Membrane	R_{NaCl} (%)	J_{NaCl} ($\text{l m}^{-2} \text{h}^{-1}$)	Testing condition	Ref.
PCNFM3	60.7	20.6	1 gL^{-1} NaCl; 25 °C; 0.6 MPa	30
NF-7	37.6	21.3	1 gL^{-1} NaCl; 25 °C; 0.6 MPa	31
PPO	36.0	63.0	1 gL^{-1} NaCl; 25 °C; 0.35 MPa	32
QAPPESK	31.0	54.0	1 gL^{-1} NaCl; 25 °C; 0.4 MPa	33
MO-6	55.4	52.13	1 gL^{-1} NaCl; 25 °C; 0.9 MPa	This work
MO-5	42.8	54.9	1 gL^{-1} NaCl; 25 °C; 0.9 MPa	
MO-4	39.2	57.5	1 gL^{-1} NaCl; 25 °C; 0.9 MPa	
MO-3	27.6	61.15	1 gL^{-1} NaCl; 25 °C; 0.9 MPa	

weight loss was observed. First step weight loss (2–5%) occurred at 100–200 °C and indicated sufficient bounded water content in the membrane matrix. Second step weight loss at 320 °C confirmed disintegration of organic segment. After 450 °C, about 10–20% residue weight was assigned for silica in membrane matrix. Hybrid membrane with comparatively high APDSMO content (MO-6) showed early weight loss in comparison to membranes with low APDSMO content (MO-5 and MO-3) because of high extent of phosphonic acid group.

DSC curves for MO-6 membrane under N_2 environment confirmed its 107 °C, T_g value (Fig. S7 ESI†), while T_g for pristine PVA was reported at 78 °C.²⁹ Hybrid membrane exhibited good mechanical stability under experimental conditions without any breaking or elongation (Fig. S8 ESI†). Chlorine tolerant nature of hybrid membrane was assessed in terms of weight loss after treatment of membrane in 5% $\text{NaClO}(\text{aq})$ solution for different time intervals (0–72 h) (Fig. S9 ESI†). Weight loss for hybrid membrane increased with silica content due to increased functionality. Moreover, no appreciable weight loss was exhibited by hybrid membranes after 25 h treatment. Acid stability of membrane was also investigated by weight loss of membrane in equilibrium with HCl and H_2SO_4 (1–8 M) for 30 days (Fig. S10 ESI†). Membrane showed about 0–4% weight loss in equilibrium with 4 M HCl or 5 M H_2SO_4 , while weight loss was remarkably higher with increased acid strengths. Also, weight loss increased with silica content in the membrane matrix. Solvent resistivity of hybrid membrane was evaluated by their weight loss under different solvent environments for 30 days (Fig. S11 ESI†). About 1.9–7.0% weight loss in 30 days under different environments (NMP, DMSO, DMF and THF), confirmed solvent stable nature of these membranes.

Water uptake, ion-exchange capacity, surface charge density

Detailed methodology used for estimation of water uptake, ion-exchange capacity (IEC), and surface charge density are included in section S2–S4 (ESI†). Membrane water uptake values increased with APDSMO content in membrane matrix (Table 1 and Fig. S12 ESI†). Water uptake depends on membrane porosity and hydrophilic nature. Degree of cross-linking enhanced with APDSMO content in the membrane matrix (reduction in PVA content). Further, phosphorylation occurred at inorganic segment (silica) thus membrane with high silica (APDSMO) content was expected to exhibit more water content. This observation was further verified by IEC values for different hybrid membranes. IEC values increased with APDSMO content

because of exchangeable phosphonic acid functional groups in the membrane matrix (Table 1). Values of membrane void porosity (τ) and surface charge density (χ^m) presented in Table 1, also support the above observation.

Membrane flux and salt rejection

Membrane flux for three different solvents (water, methanol, and hexane) was measured in a homemade stainless steel module containing two compartments separated by a circular piece of membrane. Solvents were chosen with decreasing dielectric constant Flux for different hybrid membranes under similar experimental conditions varied as: water > methanol > hexane (Fig. 6a), in similar fashion to dielectric constant. Also, membrane flux decreased with APDSMO (silica) content in the membrane, which may be attributed to a relatively high extent of cross-linking (low PVA content), which leads to compact membrane structure. Membrane flux data for different solvents, confirm high membrane permeability of polar solvents. Membrane flux increased with applied pressure (0.62–0.9 MPa) for 1 g L^{-1} NaCl solution, while salt rejection values reduced (Fig. 6b). While membrane flux decreased with silica content because of relative increase in extent of cross-linking. Salt rejection followed the opposite trend, as expected. Variation of membrane flux and salt rejection with NaCl concentrations (1–3 g L^{-1}) at constant applied pressure (0.9 MPa) confirms reduction in flux and salt rejection with feed NaCl solution concentration

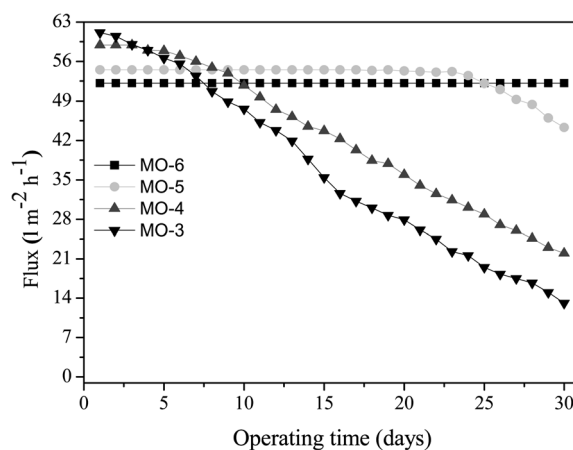


Fig. 8 Membrane flux for different time period in bacterial environment (LB media; feed solution 2.3299 OD at 600 nm) at 0.9 MPa applied pressure.

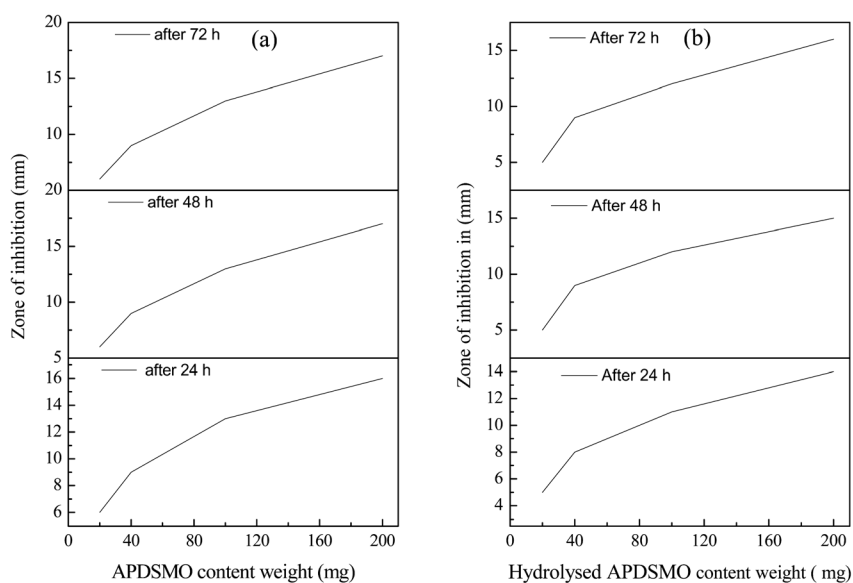


Fig. 9 Bacterial zone of inhibition (mm) with different amount of (a) siloxane (APDSMO); and (b) hydrolysed APDSMO.

(Fig. 7). This phenomenon also can be explained by osmotic pressure of salt solution. Variation of flux and salt rejection with silica content in the membrane matrix helps us to tailor the desired type of nanofiltration membranes.

Comparative performance data for different reported membranes in the literature and prepared membranes (Table 2) indicate the potential of prepared hybrid membrane, especially MO-6, for high flux and salt rejection. Membranes chlorine

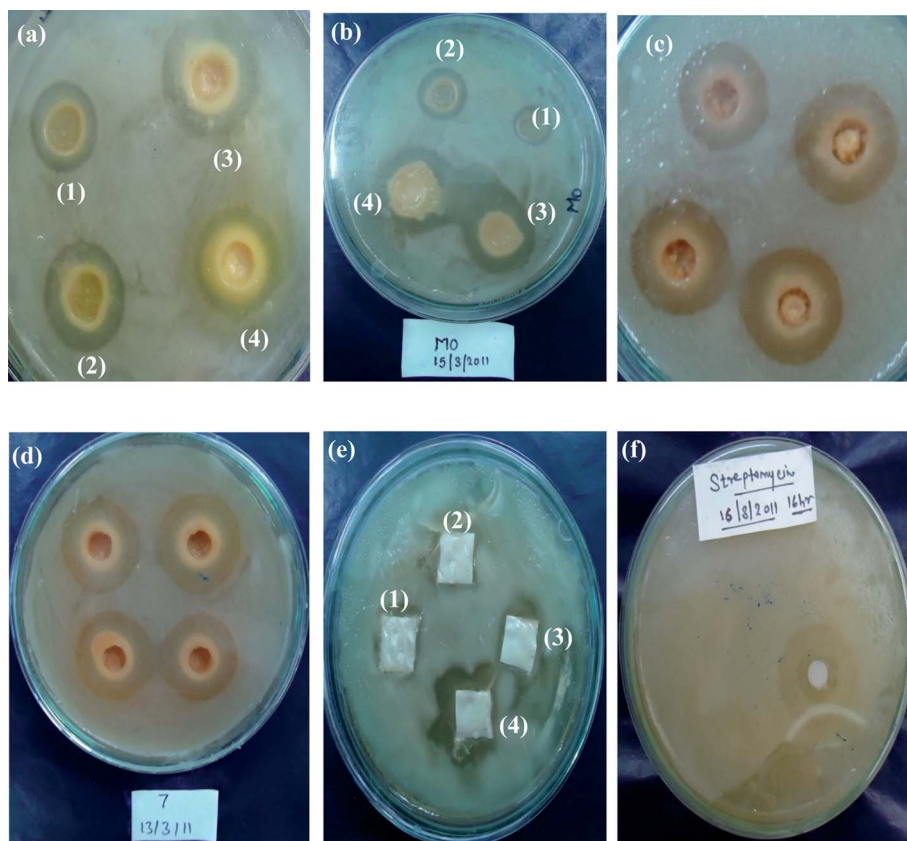


Fig. 10 Bacterial zone of inhibition of (a) APDSMO (1) 20 mg (2) 40 mg (3) 100 mg (4) 150 mg; (b) polysiloxane (1) 20 mg (2) 40 mg (3) 100 mg (4) 150 mg; (c) APDSMO, 200 mg; (d) MO-10, 200 mg; (e) Membrane (1) MO-3 (2) MO-4 (3) MO-5 (4) MO-6; (f) streptomycin.

Table 3 Antimicrobial data of siloxane (APDSMO), hydrolysed APDSMO, and polymeric membrane

Compound/Membranes	<i>A. niger</i>				<i>E. coli</i>				Zone of inhibition (mm) in 200 mg			MIC($\mu\text{g ml}^{-1}$)
	% Growth inhibition in $\mu\text{g ml}^{-1}$								24h	48h	72h	
	5000	1000	100	10	5000	1000	100	10				
APDSMO	100	80	30	10	100	72	40	20	14	16	16	3000
Hydrolysed APDSMO	96	71	24	5	94	74	35	13	12	14	15	5000
MO-6	—	—	—	—	—	—	—	—	3	4	4	9000
PVP ^a	—	—	—	—	—	—	—	—	—	—	—	10000
Standard	100	100	100	100	100	100	100	100	22	24	24	>2.0

^a PVP represents polyvinyl pyridine (Ref. 33).

tolerant nature was assessed by the flux and rejection performance of their treatment in NaOCl solution (5000 ppm) 24 h at 30 °C. Data reveal that after chlorine treatment membrane performance was unaffected, maybe due to acetylated PVA and chemically inert silica. In addition, solvent resistive and stable nature for prepared hybrid membranes is an attractive feature. Short term stability tests for prepared hybrid membranes were performed at 0.9 MPa operating pressure with *E. coli* broth solution (Fig. S13 ESI†). Obtained results depicted in Fig. 8, reveal that membranes maintained their permeability after 30 days operation. Thus, prepared hybrid membranes, especially MO-6 membrane, possessed excellent stability, and effective antibiofilm activity.

Microbial analysis

Antimicrobial properties of APDSMO, polysiloxane and prepared hybrid membranes were tested against waterborne fungi (*Aspergillum niger*) and bacteria (*Escherichia coli*).

Standard testing protocol for water insoluble and soluble antimicrobials was used.²⁶ Five different samples with varied weight of APDSMO (20–200 mg), were used for determination of bacterial zone of inhibition. Obtained results are graphically systematized in Fig. 9, while original pictures are included in Fig. 10. APDSMO showed high growth inhibiting capacity, MO-3 hybrid membrane showed minimum growth inhibition. The MO-6 hybrid membrane (high APDSMO content) exhibited good antimicrobial properties to avoid the bio-film formation on membrane surface. Single membrane piece was used six times to check the membrane long-lasting properties. It was observed that MO-6 hybrid membrane reproduced same results, during each study. Interestingly, APDSMO showed better activity than hydrolysed APDSMO. MIC values for APDSMO was less than 3000 $\mu\text{g ml}^{-1}$, while for hydrolysed APDSMO it was in between 3000–5000 $\mu\text{g ml}^{-1}$. MIC value for MO-6 hybrid membrane was 9000 $\mu\text{g ml}^{-1}$, which is lower than MIC value for poly vinyl pyridine.³³ In order to explore bacteriostatic or bactericidal nature of APDSMO, hydrolysed APDSMO, and

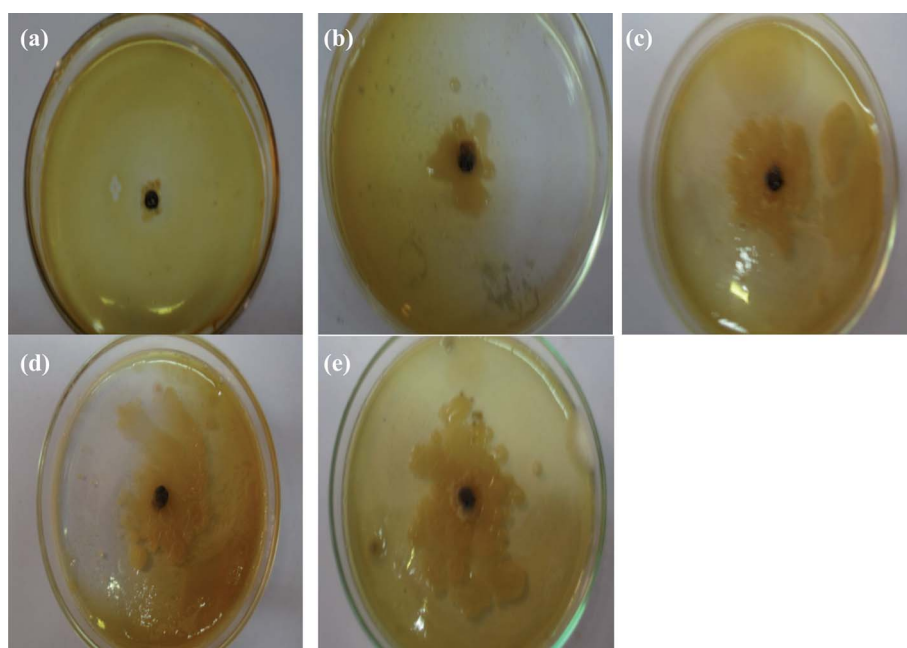


Fig. 11 Antifungal activity of *A. niger* in different concentrations of APDSMO (a) 5000 $\mu\text{g ml}^{-1}$ (b) 1000 $\mu\text{g ml}^{-1}$ (c) 100 $\mu\text{g ml}^{-1}$ (d) 10 $\mu\text{g ml}^{-1}$ (e) controlled plate (without APDSMO).

hybrid membranes, different weight amount of samples (10–10 000 $\mu\text{g ml}^{-1}$) were incubated with *E. coli* in aqueous LB broth for 24 h. 100 μL aliquots were placed on nutrient soft agar plates followed by incubation at 37 °C for 24 h, for bacterial colony counting. APDSMO and hydrolysed APDSMO showed bactericidal properties, while hybrid membranes exhibited bacteriostatic properties. Bacteriostatic properties were confirmed by calculating percentage growth inhibition (Table 3). APDSMO solution (5000 $\mu\text{g mL}^{-1}$) showed complete growth inhibition for microbes. Antifungal activity of APDSMO and hydrolysed APDSMO was also confirmed by reported method.³⁴ Results present in Table 2 revealed antifungal activity of APDSMO and hydrolysed APDSMO in four different concentrations (10–5000 $\mu\text{g ml}^{-1}$). At 5000 $\mu\text{g ml}^{-1}$ concentration, APDSMO and hydrolysed APDSMO, showed complete fungal growth inhibition (experimental picture included in Fig. 11). Fluconazole and streptomycin was used as reference drug for antifungal and antibacterial activity. Mechanism of antimicrobial activity for APDSMO and hydrolysed APDSMO is not known, but particle size, dipole moment, and solubility *etc.* play important roles.³⁵

Conclusions

Monomer APDSMO was synthesized by Barbier-Grignard reaction using APTEOS, and hybrid membranes with different weight content of silica (APDSMO) prepared by acid catalyzed sol–gel followed by formal cross-linking. Based on spectroscopy studies, schematic structure of hybrid membrane was proposed. Membrane with high APDSMO content, showed reduced crystalline region due to formation of Si–O–C bonds. Structural features of these phosphonic acid functionalized hybrid membranes changed with silica content in the membrane matrix, and membrane with high silica content (MO-6) showed lowest surface roughness (0.05 μm). Prepared membranes exhibited high thermal, mechanical, chemical (solvent and chlorine) stability. IEC, water content, and surface charge density values of hybrid membrane also confirmed their acidic nature. Membrane flux and salt rejection values varied with silica content (APDSMO) in the membrane matrix thus extent of cross-linking. This helps us to tailor the desired type of nano-filtration membranes. Performances of these membranes were compared with reported membrane in the literature, which suggested potential use of prepared hybrid membrane (especially MO-6) due to high flux and salt rejection. In addition, membranes retained their permeability after 30 days operation in *E. coli* broth solution, which confirmed their effective anti-bio-film forming activity.

Antimicrobial properties of hybrid membranes were tested against waterborne fungi (*Aspergillum niger*) and coliform bacteria (*Escherichia coli*), and MO-6 membrane (high APDSMO content) exhibited good antimicrobial properties to avoid the bio-film formation on membrane surface. MO-6 hybrid membrane exhibited about 9000 $\mu\text{g ml}^{-1}$ MIC value and bacteriostatic in nature.

Reported anti-fouling membranes are suitable for water desalination/purification. By optimising APDSMO (silica precursor) content and membrane cross-linking conditions, one can tailor the desired pore texture and charge density in the

membrane phase. Further studies are aimed for optimizing polymer design with better performance and minimum content of 1,3,4-oxadiazole. In addition, complete optimization of cross-linking extent for this water borne polymer is necessary for designing a best membrane with excellent performance, stability and durability.

Acknowledgements

Authors are thankful to Mr. Sourish Bhattacharya for his help during course of investigations. We acknowledge the Analytical Science Division, CSMCRI, Bhavnagar for instrumental support. Financial assistance received from the Department of Science and Technology, New Delhi (Govt. of India), by sponsoring project no. SR/S1/PC/06/2008 is gratefully acknowledged. Authors also thank the referees for their valuable comments.

References

- 1 P. Gong, Y. Yin and C. Yu, *Science*, 2011, **331**, 1264.
- 2 R. F. Service, *Science*, 2006, **313**, 1088.
- 3 I. Soroko, Y. Bhole and A. G. Livingston, *Green Chem.*, 2011, **13**, 162.
- 4 U. Beginn, G. Zipp, A. Mourran, P. Walther and M. Moller, *Adv. Mater.*, 2000, **12**, 513.
- 5 S. Y. Yang, I. Ryu, H. Y. Kim, J. K. Kim, S. K. Jang and T. P. Russell, *Adv. Mater.*, 2006, **18**, 709.
- 6 A. Akthaukul, R. F. Salinara and A. M. Myes, *Macromolecules*, 2004, **37**, 7663.
- 7 Y. Ji, Q. An, Q. Zhao, H. Chen, J. Qian and C. Gao, *J. Membr. Sci.*, 2010, **357**, 80.
- 8 H. B. Park, B. D. Freeman, Z. B. Zhang, M. Sankir and J. E. McGrath, *Angew. Chem. Int. Ed.*, 2008, **47**, 6019.
- 9 G. D. Kang, C. J. Gao, W. D. Chen, X. M. Jie, Y. M. Cao and Q. Yuan, *J. Membr. Sci.*, 2007, **300**, 165.
- 10 Y. H. Zhao, X. Y. Zhu, K. H. Wee and R. Bai, *J. Phys. Chem. B*, 2010, **114**, 2422–2429.
- 11 J. Mansouri, S. Harrisson and V. Chen, *J. Mater. Chem.*, 2010, **20**, 4567.
- 12 R. P. Schneider, L. M. Ferreria, P. Binder, E. M. Bejarana, K. P. Goes, E. Slongo, C. R. Machado and G. M. Z. Rosa, *J. Membr. Sci.*, 2005, **266**, 18.
- 13 Horii and K. Kannan, *Arch. Environ. Contam. Toxicol.*, 2008, **55**, 701.
- 14 N. Suzuki, S. Kiba, Y. Kamachi, N. Miyamoto and Y. Yamauchi, *J. Mater. Chem.*, 2011, **21**, 5338.
- 15 S. Egli, M. G. Nussbaumer, V. Balasubramanian, M. Chami, N. Bruns, C. Palivan and W. Meier, *J. Am. Chem. Soc.*, 2011, **133**, 4476.
- 16 J. W. Kim, L. U. Kim and C. K. Kim, *Biomacromolecules*, 2007, **8**, 215.
- 17 A. Kugel, B. Chisholm, S. Ebert, M. Jepperson, L. Jarabek and S. Stafslin, *Polym. Chem.*, 2010, **1**, 442.
- 18 C. Sanchez, B. Julian, P. Belleville and M. Popall, *J. Mater. Chem.*, 2005, **15**, 3559.
- 19 H. Zou, S. Wu and J. Shen, *Chem. Rev.*, 2008, **108**, 3893.
- 20 B. P. Tripathi and V. K. Shahi, *Prog. Polym. Sci.*, 2011, **36**, 945.
- 21 G. V. Suresh Kumar, Y. Rajendraprasad, B. P. Mallikarjuna, S. M. Chandrashekar and C. Kistayya, *Eur. J. Med. Chem.*, 2010, **45**, 2063.
- 22 J. P. N. Sangshetti and D. B. Shinde, *Eur. J. Med. Chem.*, 2011, **46**, 1040.
- 23 B. P. Tripathi, A. Saxena and V. K. Shahi, *J. Membr. Sci.*, 2008, **318**, 288.
- 24 H. Kirsebom and B. Mattiasson, *Polym. Chem.*, 2011, **2**, 1059.
- 25 M. Zhou, P. R. Nemade, X. Lu, X. Zeng, E. S. Hatakeyama, R. D. Noble and D. L. Gin, *J. Am. Chem. Soc.*, 2007, **129**, 9574.
- 26 V. Sambhy, M. M. MacBride, B. R. Peterson and A. Sen, *J. Am. Chem. Soc.*, 2006, **128**, 9798.
- 27 D. Gomes, J. Roeder, M. L. Ponce and S. P. Nunes, *J. Membr. Sci.*, 2007, **295**, 121.

- 28 Z. Xie, E. J. Henderson, O. D. W. Wang, J. E. Lofgreen, C. Kube, T. Scherer, P. M. Brodersen, Z. Z. Gu and G. A. Ozin, *J. Am. Chem. Soc.*, 2011, **133**, 5094.
- 29 B. P. Tripathi and V. K. Shahi, *ACS Appl. Mater. Interfaces*, 2009, **1**, 1002.
- 30 Y. Ji, Q. Anb, Q. Zhaob, H. Chena and C. Gao, *J. Membr. Sci.*, 2011, **376**, 254.
- 31 X. Z. Wei, L. P. Zhu, H. Y. Deng, Y. Y. Xu, B. K. Zhu and Z. M. Huang, *J. Membr. Sci.*, 2008, **323**, 278.
- 32 T. W. Xu and W. H. Yang, *J. Membr. Sci.*, 2003, **215**, 25.
- 33 C. Yan, S. H. Zhang, D. L. Yang and X. G. Jian, *J. Appl. Polym. Sci.*, 2008, **107**, 1809.
- 34 A. Busetti, D. E. Crawford, M. J. Earle, M. A. Gilea, B. F. Gilmore, S. P. Gorman, G. Lavery, A. F. Lowry, M. McLaughli and K. R. Seddon, *Green Chem.*, 2010, **12**, 420.
- 35 P. Ortega, B. M. Cobaleda, J. M. H. ández-Ros, E. F. Paniagua, J. S. Nieves, M. P. Tarazona, J. L. Copa-Patiño, J. Soliveri and F. J. d. l. M. R. Gómez, *Org. Biomol. Chem.*, 2011, **9**, 5238.